Bearing fault diagnosis in induction motor using continuous wavelet transform and convolutional neural networks

Rabah Boudiaf, Bouras Abdelkarim, Harida Issam
Laboratory of Electromechanical Systems, Department of Electromechanical, Faculty of Technology,
Badji Mokhtar University, Annaba, Algeria

Article Info

Article history:

Received Apr 30, 2023
Revised Aug 30, 2023
Accepted Sep 14, 2023

Keywords:

Bearing fault
CNN
CWT
Induction motor
Transfer learning

ABSTRACT

Induction motors are widely used in various industries due to their high efficiency, reliability and low cost. However, faults in these motors can lead to serious problems, such as unexpected shutdowns, decreased efficiency, and even damage to other parts of the system. Monitoring and diagnosing these faults are necessary. In this study, we propose a new approach for diagnosing bearing faults using convolutional neural network (CNN) and continuous wavelet transform (CWT). The suggested approach uses Scalograms with various CWT types as the network's input and utilizes many epochs and various batch sizes (Multi Ep-Batch) throughout the bearing fault classification training and testing phases. To assess our method, we implemented an extension of the Squeeze Net pre-trained model (transfer learning). The results show that the proposed method outperforms traditional methods in terms of accuracy and computational efficiency in detecting bearing faults. These results are based on publicly available MFPT data, and the proposed approach is compared to traditional methods. This work opens new research avenues in the field of bearing fault diagnosis and provides a promising solution for real-world applications.

Corresponding Author:

Rabah Boudiaf
Laboratory of Electromechanical Systems, Department of Electromechanical, Faculty of Technology
Badji Mokhtar University
C. P. 23000. Annaba, Algeria
Email: selmaneboudiaf@gmail.com

1. INTRODUCTION

Industrial maintenance efficiency is a key economic concern in major sectors today, where quick and efficient decision-making is essential [1]–[3]. The main challenges and sources of inefficiency are in deciding which maintenance actions to take in the event of machine malfunction, particularly when the machine is vital to the production process. Certain decisions can have severe economic consequences. Therefore, it is necessary to constantly monitor equipment and detect precursory signs of defects before they cause unexpected production stoppages and resulting economic losses [4], [5].

Vibration analysis is a frequently used method for the purpose of condition monitoring. Vibration analysis provides information about the functional state of bearings, including wear, misalignment, or other forms of degradation. This information allows for early detection and proactive measures to avoid unexpected downtime and expensive repairs. Signal processing tools, particularly in the diagnosis and prognosis stage of bearing health, play a vital role in maintenance [6]–[9]. Which time-frequency domain analysis method effectively extracts bearing vibration signal characteristics by decomposing them into frequency bands [10], [11].

In addition, sophisticated algorithms and software can help analyse this data and provide detailed information about the condition of the bearings. CNNs are a form of deep learning algorithm that has found widespread use in image and signal processing applications [12]–[15]. In recent years, several studies have combined WT and CNN in order to attain optimal precision and durability in bearing failure detection, because they can automatically learn the features of vibration signals and diagnose faults without the need to create features by hand.

Such as, a method in [16] was proposed that utilizes the orthogonal matching pursuit (OMP) algorithm for removing harmonic signals while preserving impact signals and noise. Additionally, the method employs wavelet transform (WT) to generate the time-frequency map of the signal and finally uses deformable CNN (D-CNN) to extract features and classify faults. Li *et al.* [17] proposed a method that uses wavelet packet transform (WPT) to decompose the signal into different frequency sub-bands, then selects the most informative sub-bands based on energy entropy, and finally uses CNN to extract features and classify faults.

Both methods achieved high recognition rates of 99.9% and 99.8%, respectively, under various fault modes and noise levels, demonstrating the effectiveness of combining WT and CNN for bearing fault diagnosis. Another study by [18] applied a CNN to vibration signals with different types of bearing defects and compared its performance with traditional signal processing methods. The results showed that the CNN-based method was more accurate and robust than traditional methods, demonstrating the potential of deep learning techniques for diagnosing errors.

A CNN was utilized to extract features from IM vibration signals, followed by the use of an SVM classifier for fault diagnosis [19]. The study found that the CNN-based method was more effective than traditional signal processing methods for bearing fault diagnosis, highlighting the potential of deep learning techniques in this area. Another study [20] proposed a method for detecting faults in induction motor bearings. The authors discuss the importance of early fault detection in induction motors and the limitations of traditional techniques for fault detection. The paper presents wavelet analysis as an effective method for decomposing the vibration signal of the motor into multiple frequency bands. The authors then describe the use of SVMs for classifying the features extracted from the wavelet analysis as either healthy or faulty.

However, deep learning techniques alone may not always provide optimal results in bearing fault diagnosis. These algorithms can be sensitive to noise and other types of interference, which can affect the accuracy of fault diagnosis. Therefore, it is important to combine these advanced techniques with traditional methods, such as signal processing and statistical analysis, to achieve optimal results.

In this paper, we propose a new approach for bearing fault diagnosis that combines the time-frequency analysis capabilities of continuous wavelet transform (CWT) with the feature extraction capabilities of CNNs. The proposed method provides comprehensive and accurate diagnosis of different types of bearing faults and outperforms traditional methods in terms of accuracy and computational efficiency. The datasets are based on publicly available MFPT data and demonstrate the effectiveness of the proposed approach in detecting different types of defects.

The rest of this manuscript is organized as follows. In first Section, we explain the theorical background for the proposed approach. Then, we provide a detailed description of the proposed method, including the design of the CNN and the application of CWT to the vibration signals, we also describe the MFPT bearing fault dataset and the data pre-processing steps. In section 5, we present the results and compare the proposed method with other methods. Finally, we provide concluding remarks and suggestions for future research.

2. THEORETICAL BACKGROUND

A novel and intelligent rolling bearing defect diagnosis method is presented in this work. Continuous wavelet transform converts raw vibration impulses into time-frequency representations. The time-frequency representations are then processed by a CNN to extract significant characteristics. Finally, a classifier is trained on the retrieved characteristics to construct a reliable diagnosis system. Following sections explain CWT and CNN's theoretical basis.

2.1. Time-frequency analysis using the continuous wavelet transform

Scaling and translating procedures improve signals in the continuous wavelet transform (CWT) time-frequency analysis approach. CWT is useful for presenting signal frequency evolution over time because it adapts to time-frequency signal analysis [21]. In this work, CWT is used to convert 1-dimensional time-domain data into 2-dimensional time-frequency pictures before feature extraction.

2.1.1. Bearing fault frequencies

Figure 1 depicts the construction of a rolling bearing. A fault in this bearing can cause high-frequency vibrations. Vibrations are generated when rolling elements collide with defects on the outer or inner race, or when a flaw on a rolling element contacts the outer or inner race. Figure 1 depicts the components of a rolling bearing's construction [22], [23].

$$\text{Outer race defect: } f_{or} = \frac{nf_r}{2}\left(1 - \frac{d}{D}cos\varphi\right) \tag{1}$$

$$\text{Inner race defect: } f_{ir} = \frac{nf_r}{2}\left(1 + \frac{d}{D}cos\varphi\right) \tag{2}$$

$$\text{Cage defect: } f_c = \frac{f_r}{2}\left(1 - \frac{d}{D}cos\varphi\right) \tag{3}$$

$$\text{Rolling element defect: } f_{re} = \frac{D}{2d}\left[1 - \left(\frac{d}{D}cos\varphi\right)^2\right] \tag{4}$$

In Figure 2, the geometric characteristics of a bearing are depicted, illustrating the various parameters involved. Specifically, the figure shows the number of balls n, the ball diameter d, the cage diameter D, the angles of the balls φ, and the rotational frequency of the bearing fr. These geometric characteristics are essential in understanding the design and performance of the bearing in different applications.

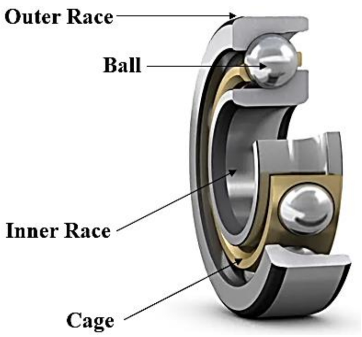

Figure 1. Diagram of the construction of a rolling bearing

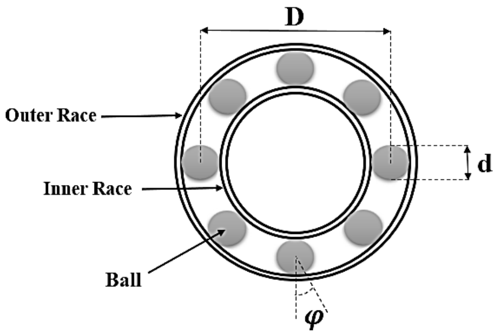

Figure 2. Geometric characteristic of a bearing

2.1.2. Continuous wavelet transforms

Data may be analysed in the time and frequency domains with the use of the continuous wavelet transform, a mathematical technique. It transforms a signal from the time domain to the time-frequency domain using wavelet functions of varying sizes and positions, resulting in coefficients that characterize the signal's frequency content across time. The CWT is useful for analysing non-stationary signals and has various applications in signal processing, image processing, and pattern recognition. The continuous wavelet transform (CWT) has reached a level of maturity, and its basic definition can be succinctly presented [24].

$$X_\omega(a,b) = \frac{1}{\sqrt{a}}\int_{-\infty}^{+\infty} x(t)\psi^*\left(\frac{t-b}{a}\right)dt \tag{5}$$

In this context, the variable a denotes the scale parameter, while b represents the time or translation parameter, the function $x(t)$ is used to denote the original one-dimensional data signal, the symbol ϕ represents the wavelet function with scale a and position offset b, and ψ^* is the complex conjugate of ψ.

2.1.3. Continuous wavelet transforms types

In the realm of fault diagnosis pertaining to induction motors (IMs), various techniques have been employed to analyze vibration signals and detect faults accurately. One widely used approach is the (CWT). Among the CWT methods, three common wavelet types have shown promise in fault diagnosis for IMs: the Morse wavelet, the Bump wavelet, and the Analytic Morlet wavelet [24], [25]. The generalized Morse wavelets are a type of analytical wavelet that are useful for analysing signals that have varying frequencies and detecting changes or discontinuities in these signals. This wavelet has several adjustable parameters, including the shape parameter ($\gamma > 0$), the oscillation control parameter ($\beta > 0$), and the order parameter

$(Z < 0)$. These parameters can be adjusted to optimize the time and frequency range for different types of signals, allowing for more accurate analysis [26]. Mathematically, the Morse wavelet can be as (6):

$$\psi_{\beta\gamma}(\omega) = \int_{-\infty}^{+\infty} \psi_{\beta\gamma}(t)\, e^{-i\omega t} dt = U(\omega) a_{\beta\gamma} \omega^{\beta} e^{-\omega^{\gamma}} \tag{6}$$

The shape parameter, denoted as β , and the time variable, denoted as t.

In the frequency domain, the bump wavelet is a band-limiting function with three adjustable settings. The time-domain variance is higher than the frequency-domain one. The ranges of practical importance for the parameters and are (3,6) and (0.1,1.2), respectively [27]. The equation for the Bump wavelet may be as (7).

$$\psi(s\omega) = e^{\left(1-\frac{1}{1-\frac{(s\omega-\mu)^2}{\rho^2}}\right)} . I_{\left[\frac{\mu-\sigma}{s}, \frac{\mu+\sigma}{s}\right]} \tag{7}$$

Where $I_{\left[\mu-\sigma/_{s}, \mu+\sigma/_{s}\right]}$ is the indicator function for the interval.

The analytic Morlet wavelet is a special case of the Morlet wavelet that has the property of being analytic, which means it has a zero mean and its positive and negative frequencies are conjugate pairs. This property makes the Analytic Morlet wavelet well-suited for analysing signals with complex structures and is commonly used in the field of time-frequency analysis. Mathematically, by dilation with a and translation with b, the Analytic Morlet wavelet family can be as (8).

$$\psi_{a,b}(t) = e^{\left[-\frac{\beta^2 (t-b)^2}{a^2}\right]} cos \left[\frac{\pi(t-b)}{a}\right] \tag{8}$$

Table 1 provides a comprehensive overview of these wavelet types and their specific characteristics for detecting faults in vibration signals from induction motors. Each of these wavelets offers unique advantages that make them well-suited for particular fault detection scenarios. For instance, the Morse wavelet is particularly effective in identifying abrupt changes in vibration signals associated with inner race and outer race faults. On the other hand, the Bump wavelet excels at detecting changes in the amplitude of vibration signals, commonly associated with rolling element faults. Lastly, the Analytic Morlet wavelet is specifically designed to analyze complex signal structures, making it a valuable tool for detecting faults in the inner race and outer race of induction motors.

By leveraging the strengths of these wavelet types, researchers and practitioners can make informed decisions regarding the selection of the most appropriate wavelet for fault diagnosis based on the specific characteristics of the signals they are analyzing [28], [29]. This, in turn, can lead to more accurate and reliable fault detection and diagnosis, contributing to improved maintenance strategies and increased operational efficiency of induction motors.

The choice of wavelet for fault diagnosis in IMs depends on the type of fault and the properties of the vibration signals. It is important to consider the unique properties of each wavelet and select the appropriate wavelet for the specific fault diagnosis scenario. By selecting the appropriate wavelet, it is possible to extract relevant features from the vibration signals and improve the accuracy and robustness of the fault diagnosis process.

Table 1. Wavelet types and their characteristics for detecting faults in vibration signals

Wavelet Type	Characteristics	Used for Detecting
Morse	Abrupt changes in signals	Abrupt changes in vibration signals (inner race and outer race faults)
Bump	Changes in amplitude of signals	Changes in amplitude of vibration signals (rolling element faults)
Analytic Morlet	Complex signal structures	Complex signal structures in vibration signals (inner race and outer race faults)

2.2. Convolutional neural network

In the field of image recognition, CNN has achieved tremendous strides [30], [31]. Figure 3 illustrates CNN's overall organizational structure. Its underlying hidden layer structure, which consists of a convolution layer, pooling layer, and fully connected layer, deep learning models greatly benefit from the utilization of a powerful tool known as data feature extraction.

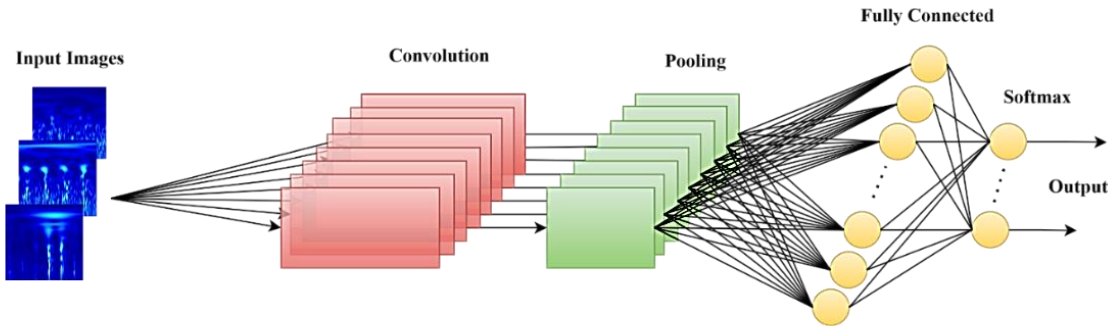

Figure 3. The CNN model's structure

2.2.1. Convolution layer

Convolutional procedures are used to produce a more sophisticated feature representation by using input data to perform local feature extraction, reducing complexity and network parameters. The following is the convolution as (9).

$$x_j^l = f\left(\sum_{i\in M_j} x_i^{l-1} k_{ij}^l + b_j^l\right) \tag{9}$$

In this context, we denote x_j^l as the output of layer l, while x_i^{l-1} represents the output of layer $l-1$, which serves as the input for layer l. The feature set of layer $l-1$ is denoted as M_j, and k_{ij}^l represents the weight matrix. Additionally, b_j^l represents the network bias, and $f\ (\cdot)$ denotes the activation function.

2.2.2. Pooling layer

Data is down-sampled at the pooling layer is typically implemented by calculating either the local average or maximum value, lowering the network's computational complexity while preserving features. The calculation method can be expressed as (10).

$$x_j^l = f\left(\beta_j^l down\left(x_j^{l-1}\right) + b_j^l\right) \tag{10}$$

Where $down\ (\cdot)$ is the down-sampling function and β indicates the network's weight.

2.2.3. Fully connected layer

The fully connected layer serves to combine feature information with category differentiation. The mathematical equation may be represented as (11).

$$y^k = f(\omega^k x^{k-1} + b^k) \tag{11}$$

In the context of neural networks, the variable k denotes the specific layer within the network. The output of the fully connected layer is denoted as y^k, while x^{k-1} represents the input to this layer. The weight coefficient is denoted as ω^k, and b^k represents the network offset.

3. THE PROPOSED APPROACH

In this manuscript, we propose a novel method that requires less time and exhibits better accuracy than the state-of-the-art methods in the training and testing phases of deep learning. In our implementation, we used scalograms and Squeeze Net with a CNN architecture to study our method, for the classification of three types of bearing faults in IMs (normal, inner race, and outer race). A flow chart of the proposed methodology for fault classification is shown in Figure 4.

All of the raw vibration signals used in this investigation were first divided into cycles. The vibration signals were then broken down into cycles using CWT, and the result was then transformed into a different 2D representation to create scalograms, which are pictures created using three different kinds of continuous wavelet transformations. The Squeeze Net deep neural network was then given these images, which had been resized to a size of 227×227 pixels in RGB format. Second, we examined the accuracy of the various CWT types by classifying the normal, inner race, and outer race vibration signals using a Squeeze Net model.

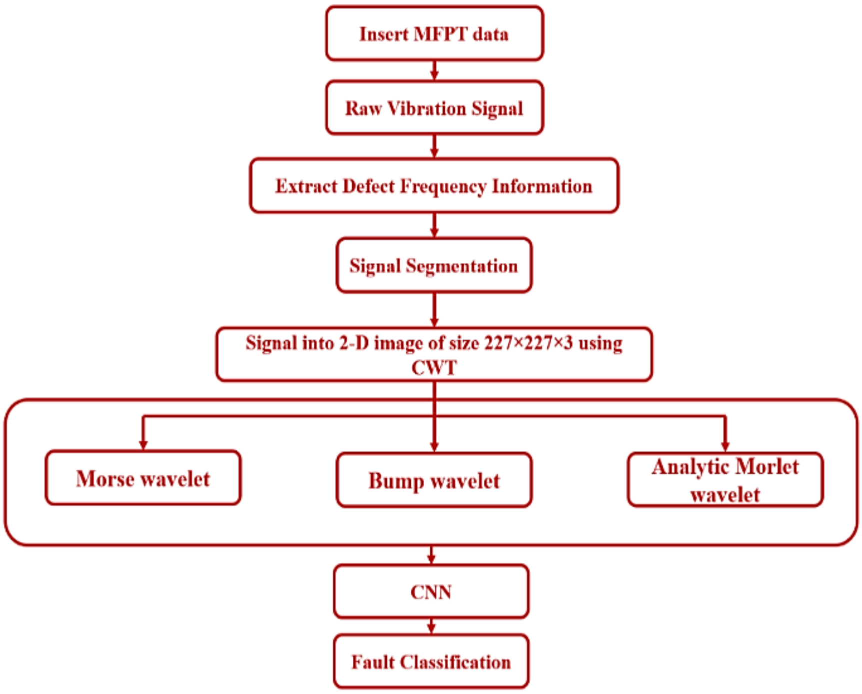

Figure 4. Flowchart for the proposed approach of fault classification.

3.1. Design of CNN

The CNN architecture commonly comprises three fundamental layers: a convolutional layer, a pooling layer, and a fully connected layer. Recently, researchers have focused on designing these layers to create various architectures for classifying vibration signals into different categories. The time domain signals are converted into 2D time-frequency spectrograms. Our technique leverages the CNN model, which uses the Squeeze Net network introduced by [32] and has three phases. First, all vibration signal segments are transformed into scalogram feature maps. The Squeeze Net network requires three 227×227×3 pictures; therefore, the photos are downsized.

The final stage of Squeeze Net's classification process involves using the 'conv10' and 'Classification Layer predictions' layers to extract image features and classify the input image. These layers combine the extracted features to generate class probabilities, predicted labels, and a loss value. To customize Squeeze Net for new image classification tasks, such as with bearing images, it is crucial to replace these two layers with new ones tailored to the specific image domain. The classification layer is responsible for determining the network's output classes, and it may be necessary to replace it with a new one that doesn't have pre-defined class labels to adapt the network for new tasks. The train network function can automatically determine the appropriate output classes for the layer during training.

3.2. The approach given for diagnosing of bearing faults

In the present study, a brand-new technique for detecting rolling bearing problems is put forward. CNNs are utilized. in this approach to enhance diagnostic performance since there is a dearth of bearing defect data accessible in practical engineering and because conventional intelligent diagnosis methods are complicated. The suggested technique is illustrated in a flowchart in Figure 4 that goes through the processes listed below:

- Step 1: Obtain vibration data from faulty bearings
- Step 2: The vibration data is first segmented and then converted into time-frequency images with dimensions of 227×227×3, using the continuous wavelet transform (CWT) techniques. The time-frequency pictures are then divided into separate sets of training and test samples, whereby each sample is assigned a corresponding label.
- Step 3: Open MATLAB and load the Squeeze Net network that has already been trained via Add-Ons. After that, feed the model the samples that were prepped in Step 2, the fully connected layer is employed in order to extract the high-level representations of features from both the training and testing images. The SoftMax function is trained using the features obtained from the training data as predictor variables.

- Step 4: The process entails inputting test samples into the trained model in order to evaluate the diagnostic accuracy.

4. EXPERIMENT MFPT DATA

This study evaluates a bearing fault diagnosis model using open-source datasets, with a focus on the MFPT dataset. The utilization of openly accessible datasets enables a thorough evaluation of the model's efficacy and improves its versatility and transparency in research. The use of MFPT data in this study enhances its credibility, allowing for thorough evaluation of the model in different fault scenarios [33].

4.1. Data description

Research and analysis of rolling bearing failures are conducted using data from the MFPT project of the society for machinery failure prevention technology. Three sets of actual fault data and three sets of experimental bearing vibration data are included in the MFPT dataset. Baseline data, inner race fault data, and outer race fault data are all included in the experiments. The reference data consists of three files, and each file contains information sampled at 97656 Hz for six seconds, for a total of 585936 samples while sustaining 270 pounds. The seven files that make up the inner race fault set were obtained by sampling at 48828 Hz for three seconds, yielding a total of 146484 samples, and subjected to loads ranging from zero to three hundred pounds. The seven files in the outer race fault set were sampled at 48828 Hz for three seconds under seven different loads ranging from 25 to 300 pounds. Deep groove ball bearings with an eight-element design, a pitch diameter of 31.62 mm, ball diameter of 5.97 mm, and contact angle are the bearings used in the experiments included in the MFPT dataset. We utilize information on bearing vibration from three sources.

4.2. Data processing

All of the data points from the three defect data sets were utilized in this experiment. The 117 segments of the three files in the baseline set each included 5000 samples. Each of the seven inner fault files had 58 segments, while each of the seven outer fault files had 117 segments. For each state, a matching number of time-frequency pictures were created by applying CWT types. A total of 234 time-frequency pictures for the first two baseline sets, 290 time-frequency photos for the first five inner race signals, and 524 time-frequency images for the outer race were acquired by combining the load circumstances for the three fault types.

Finally, as shown in Table 2, 80% of the images were chosen as training samples, and the remaining 20% were used as test samples. Figures 5 to 7 show the time-frequency images with the three types of CWT for the three conditions listed in Table 2, presented in sequence. Figure 5 displays the Morse wavelet output image, Figure 6 displays the Morlet wavelet output image, and Figure 7 displays the Bump wavelet output image. For each figure, subfigures 7(a)-7(b) represent normal condition, Figures 7(c)-7(d) represent inner race fault, and Figures 7(e)-7(f) represent outer race fault.

Table 2. Signal types, lengths, and segment numbers for training and testing data with various fault conditions

	Signals types	Signal length	Number of segments
Training	baseline_1	585936	117
	baseline_2	585936	117
	InnerRaceFault _various load 1	146484	58
	InnerRaceFault _various load 2	146484	58
	InnerRaceFault _various load 3	146484	58
	InnerRaceFault _various load 4	146484	58
	InnerRaceFault _various load 5	146484	58
	OuterRaceFault_1	585936	117
	OuterRaceFault_2	585936	117
	OuterRaceFault _various load 1	146484	58
	OuterRaceFault _various load 1	146484	58
	OuterRaceFault _various load 1	146484	58
	OuterRaceFault _various load 1	146484	58
	OuterRaceFault _various load 1	146484	58
Testing	baseline_3	585936	117
	InnerRaceFault _various load 6	146484	58
	InnerRaceFault _various load 7	146484	58
	OuterRaceFault_3	585936	117
	OuterRaceFault _various load 6	146484	58
	OuterRaceFault _various load 7	146484	58

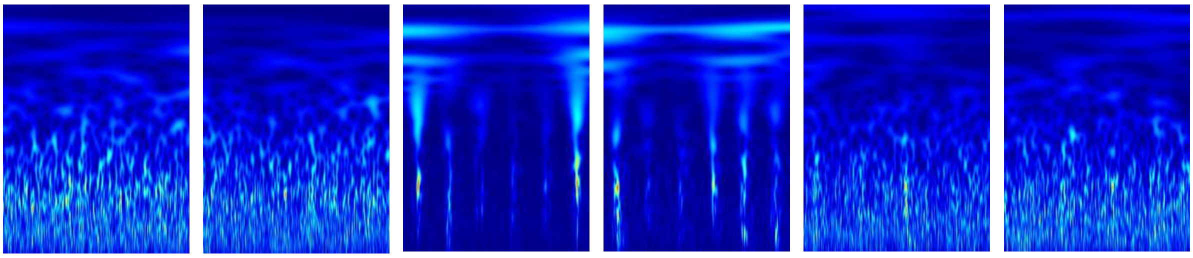

Figure 5. Morse wavelet output image (a)-(b) normal, (c)-(d) inner race fault, and (e)-(f) outer race fault

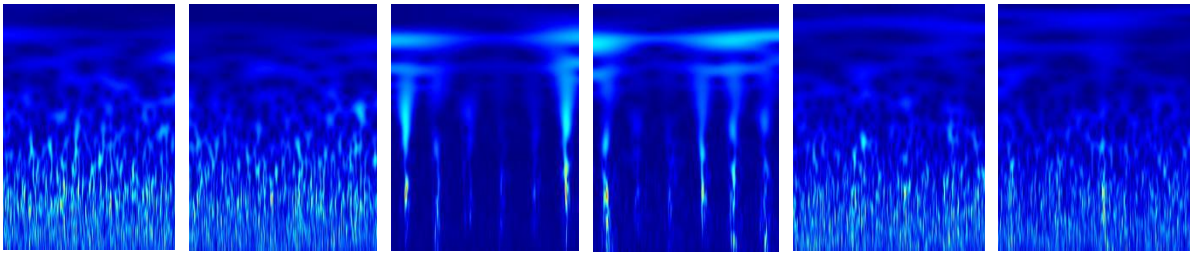

Figure 6. Morlet wavelet output image (a)-(b) normal, (c)-(d) inner race fault, and (e)-(f) outer race fault

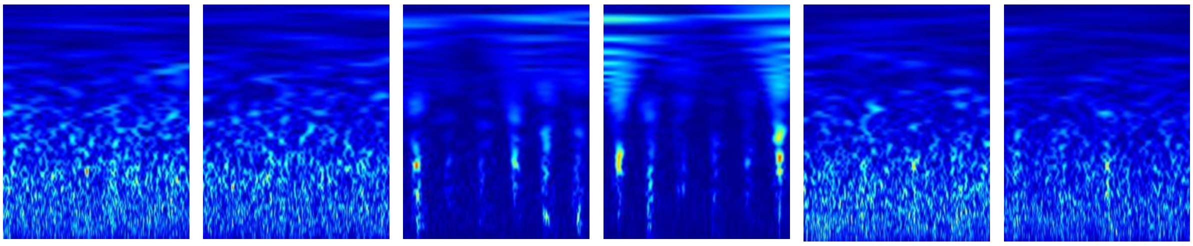

Figure 7. Bump wavelet output image (a)-(b) normal, (c)-(d) inner race fault, and (e)-(f) outer race fault

5. RESULTS AND DISCUSSION

Once the images were generated and dividing them into an 80:20 ratio for training and testing, a total of 1048 images were used for training, and 466 instances were reserved for the testing set for each type of wavelet image. The model's performance was evaluated using different parameters, namely accuracy and loss, as presented in Figures 8 to 10 for the three different wavelet images. Additionally, to gain a better understanding of the correctly and incorrectly classified instances, confusion matrices were provided in Figure 11, which is the Confusion matrix of CNN, we have provided three subfigures illustrating the results for different wavelet images. Specifically, subfigure 11(a) corresponds to the Morse wavelet, subfigure 11(b) displays results for the Morlet wavelet, and subfigure 11(c) showcases outcomes for the Bump wavelet. These subfigures offer a detailed breakdown of the model's performance for each type of wavelet image, providing valuable insights into correctly and incorrectly classified instances.

To assess a model's performance during training and testing in deep learning, accuracy and loss are two frequently used metrics. The loss measures how closely the model's predicted values match the actual values, whereas the accuracy measures how frequently the model predicts the class label of the input data correctly. The accuracy figure of a deep learning model shows how well the model performs in terms of correctly classifying the input data. It is typically represented as a percentage, where higher values indicate better performance. For example, an accuracy of 90% means that the model correctly predicted the class label of 9 out of 10 input data.

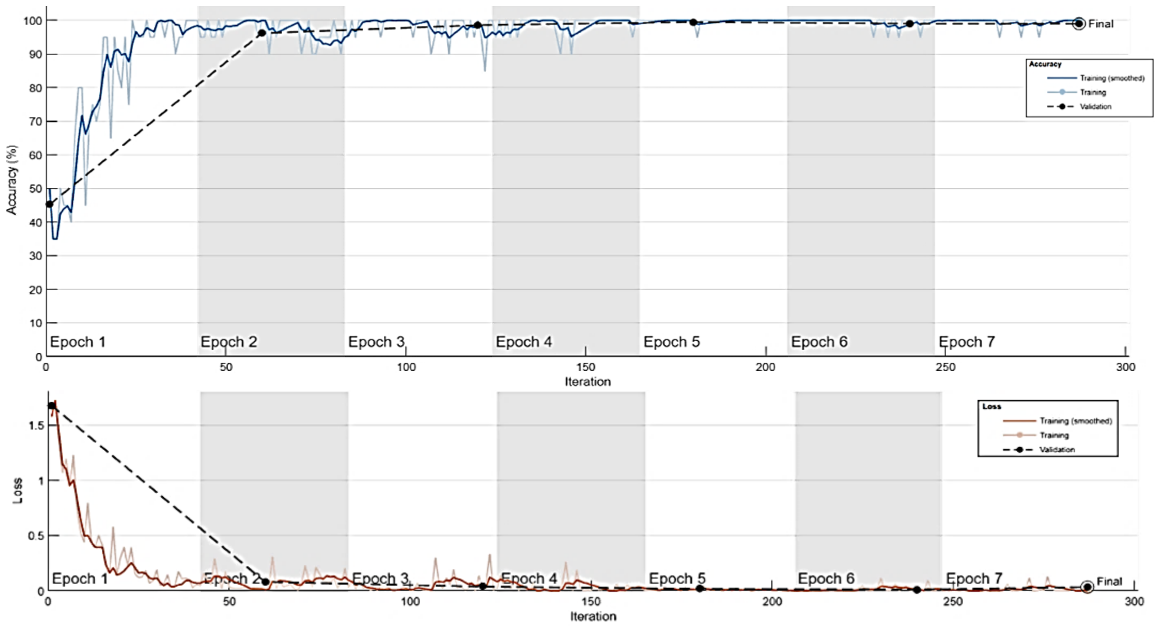

Figure 8. Performance evaluation using accuracy and loss of Morse

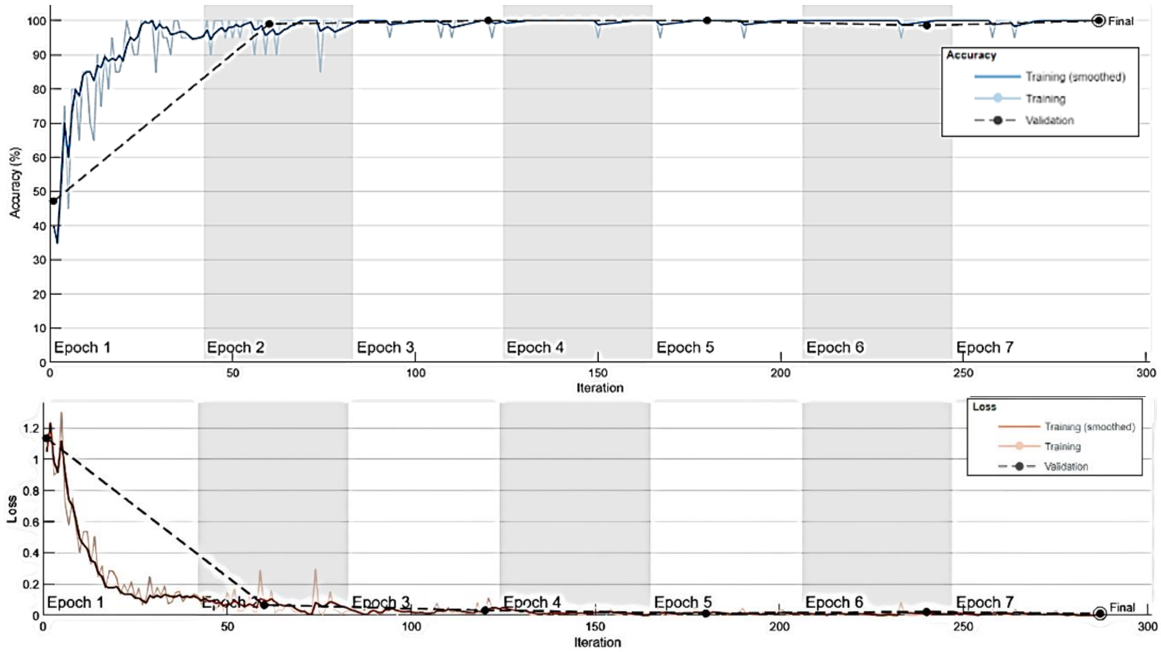

Figure 9. Performance evaluation using accuracy and loss of Morlet

On the other hand, the loss figure of a deep learning model shows how well the model's predicted values match the actual values. It is usually represented as a numerical value, where lower values indicate better performance. The loss function, which calculates the difference between predicted values and actual values, is defined based on the task at hand and the nature of the data. The reduction of the loss function is the aim of deep learning model training.

The accuracy and loss figures are used to track the model's performance during training and decide whether any changes are necessary. The model needs to be adjusted if the accuracy is poor and the loss is high, for instance by altering the architecture or hyperparameters. In contrast, the model is performing well and can be used for inference on new data if the accuracy is high and the loss is low. Overall, accuracy and loss figures offer important insights into how well a deep learning model is performing and aid in directing the development process toward a more accurate and efficient model.

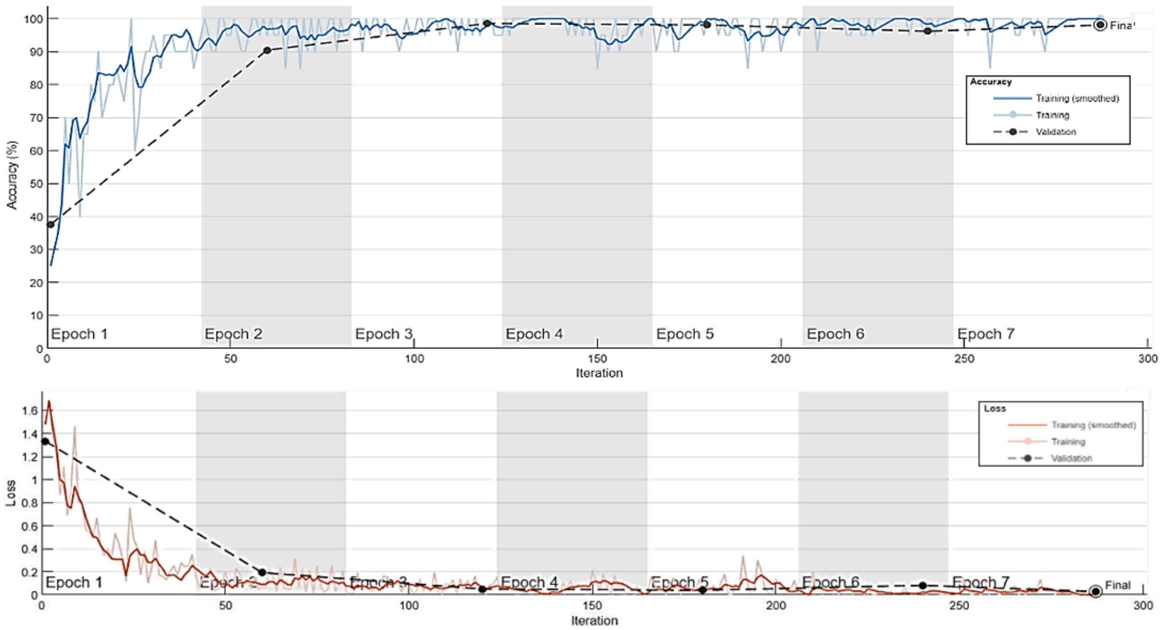

Figure 10. Performance evaluation using accuracy and loss of bump

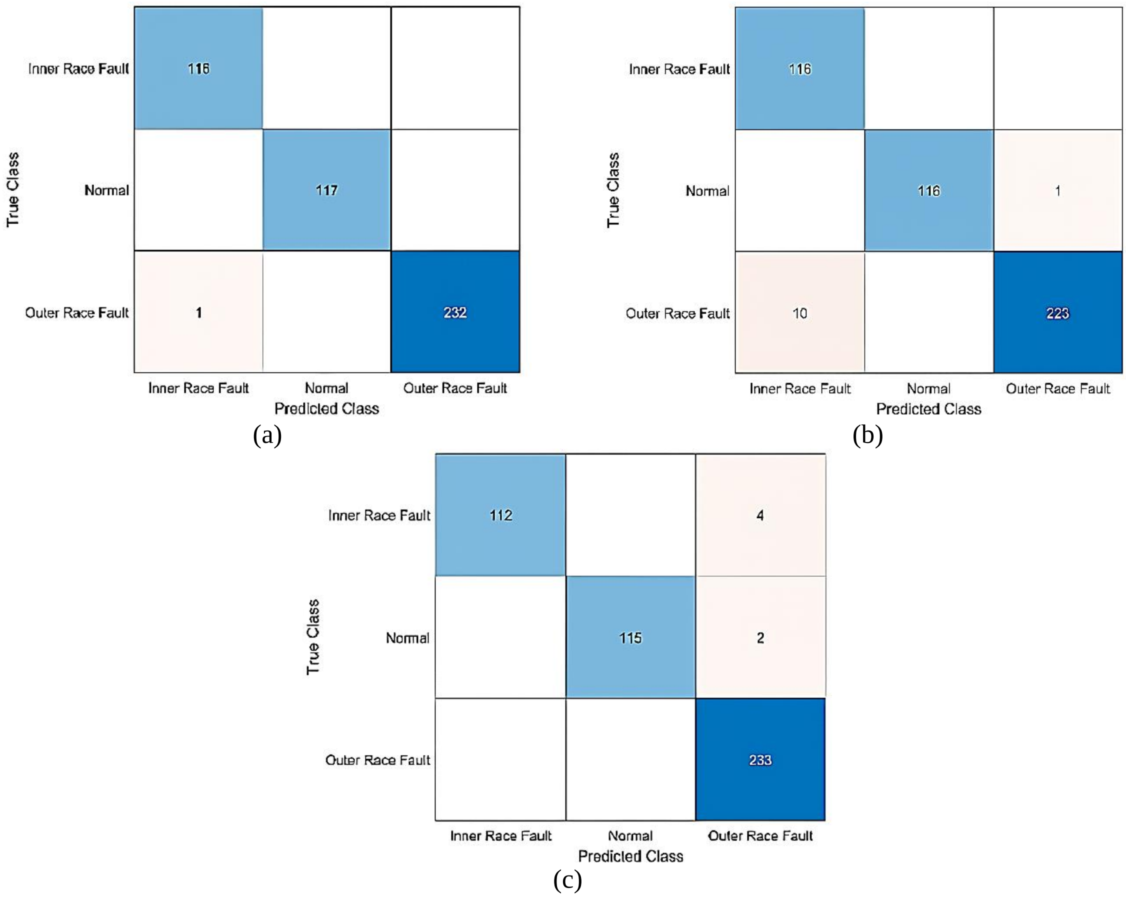

Figure 11. Confusion matrix of CNN (a) Morse wavelet, (b) Morlet wavelet, and (c) bump wavelet

By comparing the predictions of a classification model with the actual class labels of the test data, a confusion matrix is a table that is used to assess the performance of the model. Along with the number of instances of each actual class in the data, it also displays the model's percentage of correct and incorrect predictions.

The ratio of correct predictions to all of the model's predictions determines the accuracy, which measures how frequently the model correctly predicts the class label of the input data. Based on the accuracy values provided, we can compare the performance of three different classification models (Morse, Morlet, and Bump) and draw the following conclusions:

– Morse has the highest accuracy value of 99.79%, which means that it has the highest number of correct predictions compared to the other two models.
– Morlet has an accuracy value of 97.64%, which is the lowest among the three models.
– Bump has an accuracy value of 98.71%, which is higher than Morlet but lower than Morse.
– Therefore, we can conclude that Morse is the best performing model among the three models evaluated based on accuracy.

6. CONCLUSION

In conclusion, this study showcases the successful implementation of a convolutional neural network (CNN) for the accurate classification of various bearing defects based on frequency information. By utilizing three types of continuous wavelet transforms (CWTs) to convert the 1-D signal into RGB images, which were then processed by a multilayer CNN, the study achieved more than 97% accuracy in defect classification. Furthermore, the use of the pre-trained CNN model (SqueezeNet) proved effective in classifying the CWT images. This study highlights the potential for time-frequency signal representation as a feature conversion method to streamline bearing fault diagnosis in the field and pave the way for future research in this area. Ultimately, this paper presents a promising solution for real-world applications in bearing fault diagnosis.

REFERENCES

[1] E. Oztemel and S. Gursev, "Literature review of Industry 4.0 and related technologies," *Journal of Intelligent Manufacturing*, vol. 31, no. 1, pp. 127–182, Jan. 2020, doi: 10.1007/s10845-018-1433-8.
[2] J. Lee, H. D. Ardakani, S. Yang, and B. Bagheri, "Industrial Big Data Analytics and Cyber-physical Systems for Future Maintenance & Service Innovation," *Procedia CIRP*, vol. 38, pp. 3–7, 2015, doi: 10.1016/j.procir.2015.08.026.
[3] A. Bouras, S. Bouras, and S. Kerfali, "Prediction of the mass unbalance of a variable speed induction motor by stator current multiple approaches," *Turkish Journal of Electrical Engineering and Computer Sciences*, vol. 26, no. 2, pp. 1056–1068, 2018, doi: 10.3906/elk-1702-58.
[4] R. Chaïb, M. Taleb, M. Benidir, I. Verzea, and A. Bellaouar, "Failure: A source of progress in maintenance and design," *Physics Procedia*, vol. 55, pp. 185–191, 2014, doi: 10.1016/j.phpro.2014.07.027.
[5] A. Khan, S. Gupta, and S. K. Gupta, "Multi-hazard disaster studies: Monitoring, detection, recovery, and management, based on emerging technologies and optimal techniques," *International Journal of Disaster Risk Reduction*, vol. 47, 2020, doi: 10.1016/j.ijdrr.2020.101642.
[6] A. Rai and S. H. Upadhyay, "A review on signal processing techniques utilized in the fault diagnosis of rolling element bearings," *Tribology International*, vol. 96, pp. 289–306, 2016, doi: 10.1016/j.triboint.2015.12.037.
[7] Y. Lei, N. Li, L. Guo, N. Li, T. Yan, and J. Lin, "Machinery health prognostics: A systematic review from data acquisition to RUL prediction," *Mechanical Systems and Signal Processing*, vol. 104, pp. 799–834, 2018, doi: 10.1016/j.ymssp.2017.11.016.
[8] J. Zhu, N. Chen, and C. Shen, "A new data-driven transferable remaining useful life prediction approach for bearing under different working conditions," *Mechanical Systems and Signal Processing*, vol. 139, 2020, doi: 10.1016/j.ymssp.2019.106602.
[9] E. Awada, A. Al-Qaisi, E. Radwan, and M. Nour, "Motor fault detection using sound signature and wavelet transform," *International Journal of Power Electronics and Drive Systems*, vol. 13, no. 1, pp. 247–255, 2022, doi: 10.11591/ijpeds.v13.i1.pp247-255.
[10] P. K. Kankar, S. C. Sharma, and S. P. Harsha, "Rolling element bearing fault diagnosis using wavelet transform," *Neurocomputing*, vol. 74, no. 10, pp. 1638–1645, 2011, doi: 10.1016/j.neucom.2011.01.021.
[11] A. A. Alawady, M. F. M. Yousof, N. Azis, and M. A. Talib, "Frequency response analysis technique for induction motor short circuit faults detection," *International Journal of Power Electronics and Drive Systems*, vol. 11, no. 3, pp. 1653–1659, 2020, doi: 10.11591/ijpeds.v11.i3.pp1653-1659.
[12] Y. Liu, H. Pu, and D. W. Sun, "Efficient extraction of deep image features using convolutional neural network (CNN) for applications in detecting and analysing complex food matrices," *Trends in Food Science and Technology*, vol. 113, pp. 193–204, 2021, doi: 10.1016/j.tifs.2021.04.042.
[13] N. A. Dobroskok *et al.*, "Neural network based detecting induction motor defects supplied by unbalanced grid," *International Journal of Power Electronics and Drive Systems*, vol. 14, no. 1, pp. 185–198, 2023, doi: 10.11591/ijpeds.v14.i1.pp185-198.
[14] R. Jyothi, T. Holla, K. Uma Rao, and R. Jayapal, "Machine learning based multi class fault diagnosis tool for voltage source inverter driven induction motor," *International Journal of Power Electronics and Drive Systems*, vol. 12, no. 2, pp. 1205–1215, 2021, doi: 10.11591/ijpeds.v12.i2.pp1205-1215.
[15] O. Alshorman and A. Alshorman, "A review of intelligent methods for condition monitoring and fault diagnosis of stator and rotor faults of induction machines," *International Journal of Electrical and Computer Engineering*, vol. 11, no. 4, pp. 2820–2829, 2021, doi: 10.11591/ijece.v11i4.pp2820-2829.
[16] J. Guo, X. Liu, S. Li, and Z. Wang, "Bearing Intelligent Fault Diagnosis Based on Wavelet Transform and Convolutional Neural Network," *Shock and Vibration*, vol. 2020, 2020, doi: 10.1155/2020/6380486.
[17] G. Li, C. Deng, J. Wu, Z. Chen, and X. Xu, "Rolling bearing fault diagnosis based on wavelet packet transform and convolutional neural network," *Applied Sciences (Switzerland)*, vol. 10, no. 3, 2020, doi: 10.3390/app10030770.
[18] H. Y. Chen and C. H. Lee, "Deep learning approach for vibration signals applications," *Sensors*, vol. 21, no. 11, 2021, doi: 10.3390/s21113929.

[19] L. Yuan, D. Lian, X. Kang, Y. Chen, and K. Zhai, “Rolling Bearing Fault Diagnosis Based on Convolutional Neural Network and Support Vector Machine,” *IEEE Access*, vol. 8, pp. 137395–137406, 2020, doi: 10.1109/ACCESS.2020.3012053.

[20] P. Konar and P. Chattopadhyay, “Bearing fault detection of induction motor using wavelet and Support Vector Machines (SVMs),” *Applied Soft Computing*, vol. 11, no. 6, pp. 4203–4211, Sep. 2011, doi: 10.1016/j.asoc.2011.03.014.

[21] L. P. A. Arts and E. L. van den Broek, “The fast continuous wavelet transformation (fCWT) for real-time, high-quality, noise-resistant time–frequency analysis,” *Nature Computational Science*, vol. 2, no. 1, pp. 47–58, 2022, doi: 10.1038/s43588-021-00183-z.

[22] H. Saruhan, S. Saridemir, A. Çiçek, and I. Uygur, “Vibration analysis of rolling element bearings defects,” *Journal of Applied Research and Technology*, vol. 12, no. 3, pp. 384–395, 2014, doi: 10.1016/S1665-6423(14)71620-7.

[23] M. Hadjami, H. Razik, M. E. K. Oumaamar, and A. Kezzar, “Analytical model of cage induction machine dedicated to the study of the inner race bearing fault,” *International Journal of Electrical and Computer Engineering*, vol. 8, no. 1, pp. 458–471, 2018, doi: 10.11591/ijece.v8i1.pp458-471.

[24] S.-Y. Huang and Z. Bai, “Wavelets, Advanced,” *Encyclopedia of Physical Science and Technology*, pp. 753–771, 2003, doi: 10.1016/b0-12-227410-5/00939-x.

[25] J. Da Wu and J. C. Chen, “Continuous wavelet transform technique for fault signal diagnosis of internal combustion engines,” *NDT and E International*, vol. 39, no. 4, pp. 304–311, 2006, doi: 10.1016/j.ndteint.2005.09.002.

[26] J. M. Lilly and S. C. Olhede, “Generalized morse wavelets as a superfamily of analytic wavelets,” *IEEE Transactions on Signal Processing*, vol. 60, no. 11, pp. 6036–6041, 2012, doi: 10.1109/TSP.2012.2210890.

[27] A. Silik, M. Noori, W. A. Altabey, R. Ghiasi, and Z. Wu, “Comparative analysis of wavelet transform for time-frequency analysis and transient localization in structural health monitoring,” *SDHM Structural Durability and Health Monitoring*, vol. 15, no. 1, pp. 1–22, 2021, doi: 10.32604/sdhm.2021.012751.

[28] R. Yan, R. X. Gao, and X. Chen, “Wavelets for fault diagnosis of rotary machines: A review with applications,” *Signal Processing*, vol. 96, pp. 1–15, Mar. 2014, doi: 10.1016/j.sigpro.2013.04.015.

[29] Y. K. Jelbaoui, L. El Menzhi, and A. Saad, “Diagnosis of induction motor failures using discrete wavelet transform of an auxiliary winding voltage,” *Indonesian Journal of Electrical Engineering and Computer Science*, vol. 27, no. 3, pp. 1231–1241, 2022, doi: 10.11591/ijeecs.v27.i3.pp1231-1241.

[30] P. Liang, C. Deng, J. Wu, Z. Yang, J. Zhu, and Z. Zhang, “Compound Fault Diagnosis of Gearboxes via Multi-label Convolutional Neural Network and Wavelet Transform,” *Computers in Industry*, vol. 113, 2019, doi: 10.1016/j.compind.2019.103132.

[31] A. T. Radhi and W. H. Zayer, “Faults diagnosis in stator windings of high speed solid rotor induction motors using fuzzy neural network,” *International Journal of Power Electronics and Drive Systems*, vol. 12, no. 1, pp. 597–611, 2021, doi: 10.11591/ijpeds.v12.i1.pp597-611.

[32] F. N. Iandola, S. Han, M. W. Moskewicz, K. Ashraf, W. J. Dally, and K. Keutzer, “SqueezeNet: AlexNet-level accuracy with 50x fewer parameters and <0.5MB model size,” 2016.

[33] MFPT Dataset, “Society for Machinery Failure Prevention Technology,” *[Online]. Available: https://mfpt.org/fault-data-sets/*, 2012.

BIOGRAPHIES OF AUTHORS

Rabah Boudiaf received the B.Sc. and M.Sc. degrees from university 20 August 1955, Skikda, Algeria, in 2018 and 2020, respectively, all in industrial maintenance. he is currently pursuing the Ph.D. degree in industrial maintenance with department of electromechanical, Badji Mokhtar - Annaba University. His research interests include Industrial Engineering, Diagnostic and Power Systems Analysis. He can be contacted at email: selmaneboudiaf@gmail.com.

Bouras Abdelkarim received the Ph.D. degree from Badji Mokhtar-Annaba University, Algeria, in 2015, in electromechanical. currently works as academic teacher's/researcher at the Department of electromechanical, Badji Mokhtar-Annaba University. Abdelkarim does research in Industrial Engineering, Control Systems Engineering and Electrical Engineering. Their current project is Diagnostic, Renewable Energy Technologies, Electrical Power Engineering, Power Systems Analysis. He can be contacted at email: karim.bouras@hotmail.com.

Harida Issam currently works as Instrumentation Engineer at Sonatrach & pursuing the Ph.D. degree in mechatronics the with department of electromechanical, Badji Mokhtar-Annaba University. Issam does research in Industrial Engineering, Control Systems Engineering and Electrical Engineering. He can be contacted at email: issam.harida@gmail.com.